J|A|C|S
ARTICLES
Published on Web 05/25/2006

Theoretical Studies of Quantum Amplified Isomerizations for Imaging Systems Involving Hexamethyl Dewar Benzene and Related Systems

Joseph E. Norton,[†] Leif P. Olson,[‡] and K. N. Houk*,[†]

Contribution from the Department of Chemistry and Biochemistry, University of California, Los Angeles, California 90095-1569, and Research & Development, Eastman Kodak Company, Rochester, New York 14650-2109

Received January 10, 2006; E-mail: houk@chem.ucla.edu

Abstract: The ring-opening reactions of the radical cations of hexamethyl Dewar benzene (**1**) and Dewar benzene have been studied using density functional theory (DFT) and complete active-space self-consistent field (CASSCF) calculations. Compound **1** is known to undergo photoinitiated ring opening by a radical cation chain mechanism, termed "quantum amplified isomerization" (QAI), which is due to the high quantum yield. Why QAI is efficient for **1** but not other reactions is explained computationally. Two radical cation minima of **1** and transition states located near avoided crossings are identified. The state crossings are characterized by conical intersections corresponding to degeneracy between doublet surfaces. Ring opening occurs by formation of the radical cation followed by a decrease in the flap dihedral angle. A rate-limiting C_s transition state leads to a second stable radical cation with an elongated transannular C−C bond and an increased flap dihedral. This structure proceeds through a conrotatory-like pathway of C_s symmetry to give the benzene radical cation. The role of electron transfer was investigated by evaluating oxidation of various systems using adiabatic ionization energies and electron affinities calculated from neutral and cation geometries. Electron-transfer theory was applied to **1** to investigate the limiting effects of back-electron transfer as it is related to the unusual stability of the two radical cations. Expected changes in optical properties between reactants and products of Dewar benzene compounds and other systems known to undergo QAI were characterized by computing frequency-dependent indices of refraction from isotropic polarizabilities. In particular, the reaction of **1** shows greater contrast in index of refraction than that of the Dewar benzene parent system.

Introduction

Electron-transfer activation is a method of controlling various organic transformations such as symmetry-forbidden pericyclic reactions. It is well known that the rates of pericyclic reactions are often accelerated upon electron transfer[1,2] and that electron transfer is involved in several novel radical cation reactions.[3] Of specific interest here is the isomerization of hexamethyl Dewar benzene (**1**) to hexamethylbenzene (**2**), shown in Scheme 1. The radical cation-mediated rearrangement of **1** to **2** has been found to occur in a chain reaction referred to as "quantum amplified isomerization" (QAI).[4−6] In polar liquid media, electron transfer to an acceptor (**A**) in an electronic-excited electron-deficient state initiates isomerization of **1** to **2** via a chain mechanism (Scheme 2) leading to quantum yields greater than 100.[5] Since the discovery of this process in 1974, various experimental efforts have been undertaken to identify and

Scheme 1. Electron-Transfer-Induced Isomerization of Hexamethyl Dewar Benzene **1** to Hexamethyl Benzene **2**

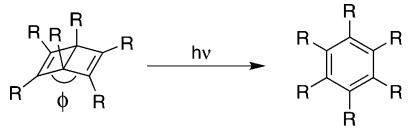

1: R = Me
3: R = H

2: R = Me
4: R = H

Scheme 2. "Quantum Amplification" Chain Mechanism for Electron-Transfer-Induced Isomerization of Hexamethyl Dewar Benzene **1** to Hexamethyl Benzene **3** in the Presence of an Acceptor (A) in Polar Solvents

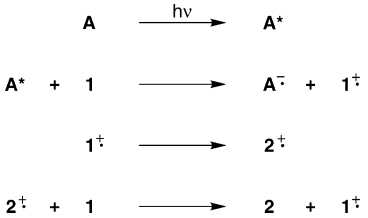

[†] University of California, Los Angeles.
[‡] Eastman Kodak Company.

(1) Bauld, N. L.; Bellville, D. J.; Harirchian, B.; Lorenz, K. T.; Pabon, R. A., Jr.; Reynolds, D. W.; Wirth, D. D.; Chiou, H. S.; Marsh, B. K. *Acc. Chem. Res.* **1987**, *20*, 371−378.
(2) Bauld, N. L. *Adv. Electron-Transfer Chem.* **1992**, *2*, 1−66.
(3) Schmittel, M.; Burghart, A. *Angew. Chem., Int. Ed. Engl.* **1997**, *36*, 2551−2589.
(4) Gillmore, J. G.; Neiser, J. D.; McManus, K. A.; Roh, Y.; Dombrowski, G. W.; Brown, T. G.; Dinnocenzo, J. P.; Farid, S.; Robello, D. R. *Macromolecules* **2005**, *38*, 7684−7694.
(5) Evans, T. R.; Wake, R. W.; Sifain, M. M. *Tetrahedron Lett.* **1973**, No. 9, 701−704.
(6) Roth, H. D.; Schilling, M. L. M.; Raghavachari, K. *J. Am. Chem. Soc.* **1984**, *106*, 253−255.

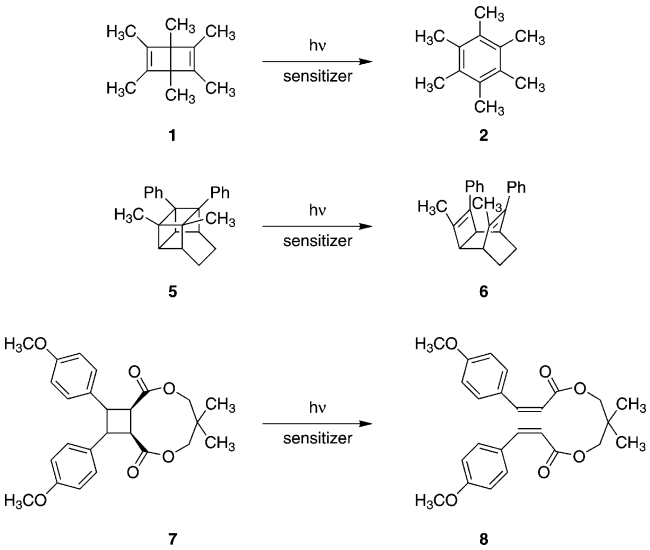

Figure 1. Systems that have been experimentally shown to undergo QAI in polymer thin films.

characterize the primary radical cation of **1**.[6−14] It was originally proposed that two distinct radical cation states of similar energy exist, namely, a $^2B_2$ (π) ground state and a less stable $^2A_1$ (σ) state.[6−8] Unfortunately, further studies have been unable to verify a $^2A_1$ state and have only provided definitive evidence of the $^2B_2$ ground state.[9−13] However, computational methods indicate that in theory two minima should exist.[6,15,16]

Several systems (Figure 1) have been shown to undergo QAI in molecularly doped polymer thin films; hexamethyl Dewar benzene appears to be the most promising QAI substrate.[4,17−20] The proposed mechanism for QAI in solid media consists of photoinitiated electron transfer from reactant to sensitizer followed by isomerization of the radical cation, propagation of ring opening by cycles of isomerization and electron transfer, and termination via a final return electron transfer. The reaction correlates spatially to light exposure because the polymer binder limits diffusion of the QAI reactant and product molecules. This permits essentially complete conversion of reactant to product in irradiated areas of the polymer film, while the nonirradiated areas contain very little product. Systems exhibiting QAI could be useful for refractive index imaging or other optical applications, such as holography, because the index of refraction of the reactant is different from that of the product. Successful high-resolution refractive-index imaging by QAI was achieved by Robello, Farid, Dinnocenzo, and co-workers,[4,17−20] demonstrating a completely processless, highly sensitive, chemically amplified procedure that exhibits negligible dimensional changes and changes in index of refraction ($\Delta n \geq 0.005$) that are suitable for many applications. In contrast to shrinking that occurs with polymer cross-linking chemistry, the volume of the reactant and product are quite similar. The QAI systems shown in Figure 1 have been experimentally investigated as refractive-index imaging systems[18] and are under investigation in the current study. Particular attention is given to the radical cation rearrangements of Dewar benzene. Systems shown in Figure 2 will be evaluated as potential systems for QAI.

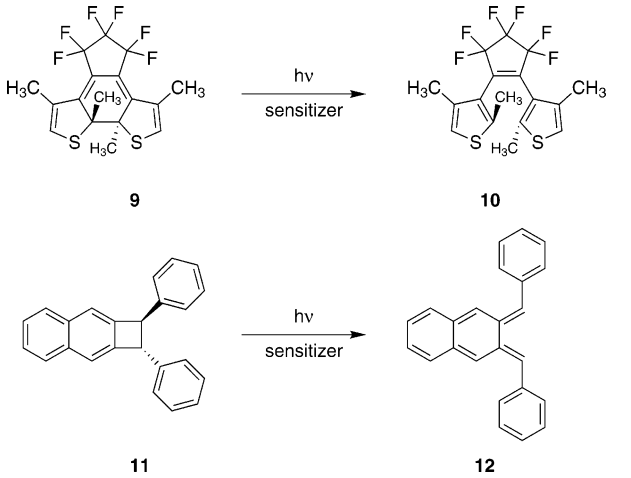

Figure 2. Potential QAI systems studied here with B3LYP/6-31G(d).

While a comprehensive understanding of the mechanistic details of pericyclic reactions of radical cations has yet to be established, significant progress toward characterizing these types of reactions has been made and is relevant to the isomerization of the radical cation of **1**.[21−29] The radical cation isomerization of the parent system Dewar benzene is reminiscent of such reactions as the ring opening of the cyclobutene radical cation,[21−26] and it should exhibit similar mechanistic features. For the cyclobutene radical cation, a flat region in the potential energy surface is attributed to weaker bonding characteristics (offering less resistance to geometrical deformations) and to the existence of low-lying excited states that favor vibronic interactions.[22] On such flat potential surfaces near transition states, it is likely that dynamic, substituent, and solvent properties heavily influence relative energetics, as previously demonstrated for such reactions as the biradical rearrangement of bicyclo[3.1.0]hex-2-ene,[30] cyclopropane stereomutation,[31−33] and the ring opening

(7) Rhodes, C. J. *J. Am. Chem. Soc.* **1988**, *110*, 4446−4447.
(8) Rhodes, C. J. *J. Am. Chem. Soc.* **1988**, *110*, 8567−8568.
(9) Peacock, N. J.; Schuster, G. B. *J. Am. Chem. Soc.* **1983**, *105*, 3632−3638.
(10) Gebicki, J.; Marcinek, A.; Mayer, J. *J. Am. Chem. Soc.* **1989**, *111*, 3098−3099.
(11) Qin, X. Z.; Werst, D. W.; Trifunac, A. D. *J. Am. Chem. Soc.* **1990**, *112*, 2026−2027.
(12) Arnold, A.; Gerson, F. *J. Am. Chem. Soc.* **1990**, *112*, 2027−2028.
(13) Williams, F.; Guo, Q. X.; Nelsen, S. F. *J. Am. Chem. Soc.* **1990**, *112*, 2028−2030.
(14) Marcinek, A. *J. Phys. Chem. A* **1998**, *102*, 7761−7764.
(15) Salhi-Benachenhou, N.; Eriksson, L. A.; Lunell, S. *Acta Chem. Scand.* **1997**, *51*, 636−640.
(16) Bews, J. R.; Glidewell, C. *THEOCHEM* **1982**, *3*, 197−204.
(17) Robello, D. R.; Farid, S.; Dinnocenzo, J.; Brown, T.; Peer, A. Quantum Amplified Isomerization: Mechanism of Photoinitiated Electron-Transfer Chain Reactions in Solid Media and Applications to Refractive Index Imaging. Sixth International Symposium on Functional π-Electron Systems, June 14−18, 2004; Cornell University, Ithaca, New York (Poster).
(18) Robello, D. R.; Dinnocenzo, J. P.; Farid, S.; Gillmore, J. G.; Thomas, S. W., III. *ACS Symp. Ser.* **2005**, *888*, 135−146.
(19) Robello, D. R.; Farid, S.; Dinnocenzo, J. P.; Gillmore, J. G. *Polym. Prepr. (Am. Chem. Soc., Div. Polym. Chem.)* **2002**, *43*, 163−164.
(20) Robello, D. R.; Dinnnocenzo, J. P.; Farid, S.; Gillmore, J. G.; Thomas, S. W., III. *Polym. Prepr. (Am. Chem. Soc., Div. Polym. Chem.)* **2001**, *42*, 717−718.
(21) Barone, V.; Rega, N.; Bally, T.; Sastry, G. N. *J. Phys. Chem. A* **1999**, *103*, 217−219.
(22) Sastry, G. N.; Bally, T.; Hrouda, V.; Carsky, P. *J. Am. Chem. Soc.* **1998**, *120*, 9323−9334.
(23) Swinarski, D. J.; Wiest, O. *J. Org. Chem.* **2000**, *65*, 6708−6714.
(24) Wiest, O. *J. Am. Chem. Soc.* **1997**, *119*, 5713−5719.
(25) Aebischer, J. N.; Bally, T.; Roth, K.; Haselbach, E.; Gerson, F.; Qin, X. Z. *J. Am. Chem. Soc.* **1989**, *111*, 7909−7914.
(26) Saettel, N. J.; Oxgaard, J.; Wiest, O. *Eur. J. Org. Chem.* **2001**, 1429−1439.
(27) Wiest, O.; Oxgaard, J.; Saettel, N. J. *Adv. Phys. Org. Chem.* **2003**, *38*, 87−109.
(28) Oxgaard, J.; Wiest, O. *J. Phys. Chem. A* **2002**, *106*, 3967−3974.
(29) Oxgaard, J.; Wiest, O. *J. Phys. Chem. A* **2001**, *105*, 8236−8240.
(30) Suhrada, C. P.; Houk, K. N. *J. Am. Chem. Soc.* **2002**, *124*, 8796−8797.
(31) Doubleday, C., Jr.; Bolton, K.; Hase, W. L. *J. Phys. Chem. A* **1998**, *102*, 3648−3658.

of substituted cyclobutene radical cations.[23] In related systems involving 1,3-butadiene radical cations, well-defined ridges observed in the potential energy surface have been attributed to rehybridization effects caused by the radical cation.[28] These studies describe rather regularly encountered characteristics of pericyclic reactions involving radical cations. The combination of a highly strained structure and formation of a radical cation in **1** could lead to bond weakening of the bridge, flattening of the potential energy surface, and symmetry-breaking effects.

Computational efforts, thus far, have provided limited characterization of the radical cation of **1**. Ab initio calculations on hexamethyl Dewar benzene have provided evidence of two distinct radical cation states where the $^2B_2$ state is more stable than the $^2A_1$ state.[6] Calculations performed using MINDO/3 give the opposite prediction, with the $^2A_1$ state being the minimum-energy geometry.[16] More recent studies with DFT methods have also predicted the $^2B_2$ state to be the ground state[15] and have shown that upon removal of one electron from the π system a large distortion of the flap dihedral of **1** occurs, contributing significantly to experimentally observed reorganization energies.[34] Currently, computational studies have not been performed with efforts to identify transition states or explain the relative stability of the different radical cation states and the observed changes in flap dihedral angles.

In the current study, we provide a computational description of the potential energy surface for the neutral and radical cation rearrangement of **1** to **2** and evaluate other systems as potentially good candidates for QAI. The aim is to establish the electronic structures involved in the isomerization of $\mathbf{1}^{\bullet+}$ to $\mathbf{2}^{\bullet+}$ and to consider this process in the context of quantum amplification. The properties obtained directly from computational methods such as nuclear reorganization energy, molecular volume, and redox potentials are used to calculate rate constants for electron transfer. From this, one can comment on kinetically favored processes and events that might limit or hinder the efficiency of QAI involving **1**. Specifically, the rates of electron transfer between donor **1** and excited electron acceptor **A*** and the energetics of the propagation step, i.e., electron transfer between **1** and $\mathbf{2}^{\bullet+}$, can be compared to the isomerization process of $\mathbf{1}^{\bullet+}$ and back-electron-transfer events. In this way, electronic structure calculations provide insight into quantum amplification of isomerization.

Computational Methods

All calculations were carried out using the Gaussian 03 software package.[35] DFT calculations were performed using the Becke3LYP[36,37] functional with 6-31G(d) and 6-311+G(d,p) basis sets. Complete active-space self-consistent field (CASSCF/6-31G(d)) calculations on Dewar benzene and hexamethyl Dewar benzene were performed using a 6-electron, 6-orbital (6,6) active space for neutral ground states and a 5-electron, 6-orbital (5,6) active space for radical cation states. The active spaces comprise the electrons of the π and π* orbitals of benzene and hexamethylbenzene or the π and π* orbitals and transannular C−C σ and σ* orbitals of Dewar benzene and hexamethyl Dewar benzene. Conical intersections, nonadiabatic derivative coupling (DC) vectors, and gradient difference (GD) vectors were calculated using the algorithm of Bearpark et al.[38] implemented in Gaussian 03.[35]

Full geometry optimizations and analytical vibrational frequency analyses were carried out for all stationary and transition structures. Ground-state structures were found to be minima with zero imaginary frequencies, while transition structures were found to be first-order saddle points with a single imaginary frequency corresponding to vibration along the appropriate reaction coordinate.

Contour plots of potential energy surfaces of Dewar benzene and hexamethyl Dewar benzene were carried out using the scan function available in Gaussian 03.[35] Each point represents an optimized structure with the indicated geometric constraints along the specified reaction coordinates. A total of 442 optimized structures were calculated for each surface.

Electron-transfer rates were calculated using the following equations based on Marcus theory[39,40] and other related well-known electron-transfer theories[41−45]

$$k = \left(\frac{4\pi^3}{h^2\lambda_s k_B T}\right)^{1/2} |V|^2 \sum_{w=0}^{\infty}\left(\frac{e^{-S}S^w}{w!}\right) \exp\left\{-\frac{(\lambda_s + \Delta G + wh\upsilon)^2}{4\lambda_s k_B T}\right\} \quad (1)$$

$$S = \frac{\lambda_v}{h\upsilon} \quad (2)$$

where V, λ_s, λ_v, ν, and ΔG are the electron-coupling matrix element, solvent reorganization energy, vibration reorganization energy, single average frequency, and free energy change for the electron-transfer process, respectively. The parameters for electron-transfer equations were obtained either from electronic structure calculations or experimentally known values.[46,47] The terms h, k_B, and T are the Planck constant, Boltzmann constant, and temperature, respectively.

Indices of refraction were calculated using the Lorentz−Lorenz equation.[48−52]

$$n(\omega) = \sqrt{\frac{3 + 8\pi N\alpha(\omega)}{3 - 4\pi N\alpha(\omega)}} \quad (3)$$

This form of the Lorentz−Lorenz expression requires the frequency-dependent polarizability, $\alpha(\omega)$, and the number of molecules per unit volume, N. Polarizability is quantum mechanically calculated as a tensor quantity in terms of its individual tensors. The index of refraction of interest for amorphous materials, such as organic liquids, is the average isotropic polarizability. Values of N can be determined from the density of experimentally known systems or can be approximated computa-

(32) Doubleday, C., Jr.; Bolton, K.; Hase, W. L. *J. Am. Chem. Soc.* **1997**, *119*, 5251−5252.
(33) Hrovat, D. A.; Fang, S.; Borden, W. T.; Carpenter, B. K. *J. Am. Chem. Soc.* **1997**, *119*, 5253−5254.
(34) Kiau, S.; Liu, G.; Shukla, D.; Dinnocenzo, J. P.; Young, R. H.; Farid, S. *J. Phys. Chem. A* **2003**, *107*, 3625−3632.
(35) Frisch, M. J.; et al. *Gaussian 03*; Gaussian, Inc.: Wallingford, CT, 2004.
(36) Lee, C.; Yang, W.; Parr, R. G. *Phys. Rev. B: Condens. Matter Mater. Phys.* **1988**, *37*, 785−789.
(37) Becke, A. D. *J. Chem. Phys.* **1993**, *98*, 5648−5652.
(38) Bearpark, M. J.; Robb, M. A.; Schlegel, H. B. *Chem. Phys. Lett.* **1994**, *223*, 269−274.
(39) Marcus, R. A. *J. Chem. Phys.* **1956**, *24*, 966−978.
(40) Marcus, R. A.; Eyring, H. *Annu. Rev. Phys. Chem.* **1964**, *15*, 155−196.
(41) Van Duyne, R. P.; Fischer, S. F. *Chem. Phys.* **1974**, *5*, 183−97.
(42) Ulstrup, J.; Jortner, J. *J. Chem. Phys.* **1975**, *63*, 4358−68.
(43) Siders, P.; Marcus, R. A. *J. Am. Chem. Soc.* **1981**, *103*, 741−747.
(44) Siders, P.; Marcus, R. A. *J. Am. Chem. Soc.* **1981**, *103*, 748−752.
(45) Miller, J. R.; Beitz, J. V.; Huddleston, R. K. *J. Am. Chem. Soc.* **1984**, *106*, 5057−5068.
(46) *Mathematica*, Version 4.0; Wolfram Research, Inc.: Champaign, IL, 1999.
(47) Application of electron-transfer theory also includes use of the Rehm−Weller equation, Marcus theory for electron transfer and solvent reorganization energies, and calculation of redox potentials. For computational details and relevant references for the procedures used in this study, see Supporting Information.
(48) Lorentz, H. A. *The Theory of Electrons*; Dover: New York, 1952.
(49) Böttcher, C. J. F. *Theory of Electric Polarization*, 2nd ed.; Elsevier: Amsterdam, 1973.
(50) Nussbaum, A.; Phillips, R. A. *Contemporary Optics for Scientists and Engineers*; Prentice Hall: Englewood Cliffs, NJ, 1976.
(51) Sylvester-Hvid, K. O.; Astrand, P.-O.; Ratner, M. A.; Mikkelsen, K. V. *J. Phys. Chem. A* **1999**, *103*, 1818−1821.
(52) Sylvester-Hvid, K. O.; Mikkelsen, K. V.; Ratner, M. A. *J. Phys. Chem. A* **1999**, *103*, 8447−8457.

Table 1. . Calculated Relative Energies for Dewar Benzene Ground and Radical Cation States at the CAS and (U)B3LYP Levels of Theory[a]

	Dewar benzene		
	CAS/6-31G(d)	(U)B3LYP/6-31G(d)	6-311+G(d,p)
DB	84.3	84.3	84.8
π RC	278.9	278.3	284.9
$\pi-\sigma$ TS	281.8[b]	286.3	292.3
σ RC	273.1	281.1	286.5
CTS	273.1[c]	282.7	287.7
BRC	188.0	204.3	210.6
B	0.0	0.0	0.0
CI ($\pi-\sigma$)	296.1	–	–
CI (CTS)	276.0	–	–

[a]Energies are reported in kcal/mol. [b] $\Delta E = 290.3$ using equally weighted state averaging over the two lowest roots. [c] $\Delta E = 274.8$ using equally weighted state averaging over the two lowest roots.

Table 2. Calculated Relative Energies for Hexamethyl Dewar Benzene Ground and Radical Cation States at the CAS and (U)B3LYP Levels of Theory[a]

	hexamethyl Dewar benzene			
	CAS/ 6-31G(d)	(U)B3LYP/ 6-31G(d)	(U)B3LYP/ 6-311+G(d,p)	experimental
HMDB	56.0	60.1	59.3	59.4 ± 2.1
π RC	223.2	222.1	225.7	
$\pi-\sigma$ TS	228.2[b]	230.2	233.3	
σ RC	221.5	227.6	230.4	
CTS	222.0[c]	230.1	232.6	
BRC	159.9	169.6	173.7	
HMB	0.0	0.0	0.0	
CI ($\pi-\sigma$)	242.0	–	–	
CI (CTS)	226.8	–	–	

[a] Energies are reported in kcal/mol. [b] $\Delta E = 236.2$ using equally weighted state averaging over the two lowest roots. [c] $\Delta E = 224.1$ using equally weighted state averaging over the two lowest roots.

tionally. The GRASP program[53] was used to determine N where experimental data were lacking.[54]

Results and Discussion

Exploration of Potential Energy Surfaces. As the first part of this study, we have examined the neutral ground state and radical cation potential energy surfaces of hexamethyl Dewar benzene (**1**) and its parent system, Dewar benzene (**3**). Upon oxidation of **1** and **3**, isomerization of the bicyclic radical cation gives the benzene radical cation that subsequently oxidizes other reactant molecules. The critical points and potential energy surfaces related to radical cation isomerization have been explored using DFT and CASSCF methods. In the accompanying paper by Bally, Matzinger, and Bednarek (BMB), the ground state of the radical cation of the parent system **3** was studied in detail, and considerable attention was given to the correlation of orbital and state symmetries.[55] Our calculations clearly establish the lowest-energy potential energy surface for both **1** and **3**, and relevant critical points are investigated and are entirely consistent with the results of BMB.[55] We refrain from going into extensive detail on points covered thoroughly by BMB.

Consistent with previous computational studies,[6,15,16] the radical cation of hexamethyl Dewar benzene and Dewar benzene are both found to have two true minima. One of these is the $^2B_2$ state with an electron localized on the double bonds, a transannular C−C bond that is not much altered from the neutral molecule and a decrease in the flap dihedral, ϕ. The other minimum is a $^2A_1$ state where an electron is localized on the transannular C−C bond, resulting in a quite stretched but not fully broken σ bond and a relatively unchanged flap dihedral compared to that of the ground-state geometry. Similar stationary points and transition structures were identified with each level of theory. The relative energies for calculated structures are listed in Tables 1 and 2, with corresponding structures shown in Figures 3 and 4, respectively. The potential energy surface for the ring-opening reaction of hexamethyl Dewar benzene is shown in Figure 5.

Structures found for **1** closely resemble those found for **3**. Upon oxidation, both systems relax to π **RC** with a $^2B_2$ radical cation state. For Dewar benzene systems, (U)B3LYP/6-311+G(d,p) and CAS/6-31G(d) predict a decrease in ϕ, ranging from 117 to 118° to 104−109° and from 116° to 104−108°. The transannular C−C bond lengths remain relatively unchanged, and the oxidized π bonds become slightly longer. π **RC** is connected to σ **RC** by a transition structure located near an avoided crossing, $\pi-\sigma$ **TS**, that has activation energy of ∼5−8 kcal/mol for **1** and ∼3−8 kcal/mol for **3**. State averaging over the lowest two roots places the CAS barriers even higher at 13 kcal/mol for **1** and 11 kcal/mol for **3**. Structure σ **RC** corresponds to the $^2A_1$ radical cation state where the electron deficiency migrates from the π bonds to the transannular C−C bond resulting in a very elongated σ bond. For **3**, the C−C σ bond lengthens from 1.58 to 1.70 Å with (U)B3LYP/6-311+G(d,p) and from 1.62 to 1.77 Å with CAS/6-31G(d). For **1**, the C−C σ bond extends from 1.59 to 1.74 Å with (U)B3LYP/6-311+G(d,p) and 1.62 to 1.82 Å with CAS/6-31G(d). For both systems, σ **RC** experiences C−C bond elongation and an increase in ϕ to a value close to that of the neutral state that allows the structure to become more planar.

For **1**, CAS/6-31G(d) predicts σ **RC** to be 1.7 kcal/mol more stable in energy than π **RC**, whereas (U)B3LYP/6-31G(d) and (U)B3LYP/6-311+G(d,p) predict σ **RC** to be 5.5 and 4.7 kcal/mol less stable than π **RC**, respectively, with the same trend existing for **3**.

Isomerization of the neutral form of Dewar benzene was assumed to occur via a thermally forbidden disrotatory electrocyclic ring opening, given that the thermally allowed conrotatory pathway was thought to give the extraordinarily strained *cis*,*cis*,*trans*-cyclohexa-1,3,5-triene.[56,57] However, ab initio calculations have shown that isomerization of Dewar benzene proceeding through the conrotatory pathway leads directly to benzene.[58] The current results support these conclusions in that the conrotatory pathway never leads to the strained trans conformation in conducting surface scans of **3**. In contrast, surface scans for **1** demonstrate a preference for the conrotatory

(53) Nicholls, A.; Sharp, K.; Honig, B. *Proteins: Struct., Funct., Genet.* **1991**, *11*, 281ff.
(54) The GRASP program was used to generate a correlation between calculated molecular surface volumes (V_{GRASP}) and experimentally known condensed phase molar volumes (V_{exp}) from which values of N could be determined. A test set comprising a number of small aromatic systems was used to generate the equation, $V_{GRASP} = 1.8901$; $V_{exp} - 6.5937$ with $R^2 = 0.9789$; and RMSD = 5.87%. A detailed description of GRASP data and linear regression analysis is provided in the Supporting Information.
(55) Bally, T.; Matzinger, S.; Bednarek, P. *J. Am. Chem. Soc.* **2006**, *128*, 7828−7834.
(56) Woodward, R. B.; Hoffmann, R. *The Conservation of Orbital Symmetry*; Verlag Chemie: Weinheim, 1970.
(57) Johnson, R. P.; Daoust, K. J. *J. Am. Chem. Soc.* **1996**, *118*, 7381−7385.
(58) Havenith, R. W. A.; Jenneskens, L. W.; van Lenthe, J. H. *THEOCHEM* **1999**, *492*, 217−224.

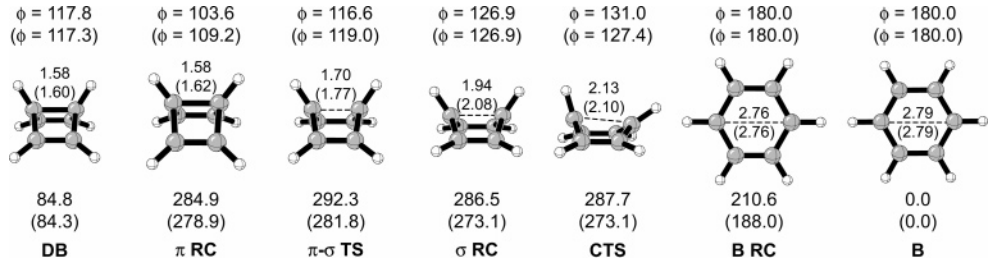

Figure 3. UB3LYP/6-311+G(d,p) Dewar benzene structures with flap dihedral, ϕ, reported in degrees, C−C bond distances reported in Å, and energies reported in kcal/mol. CAS/6-31G(d) values are shown in parentheses.

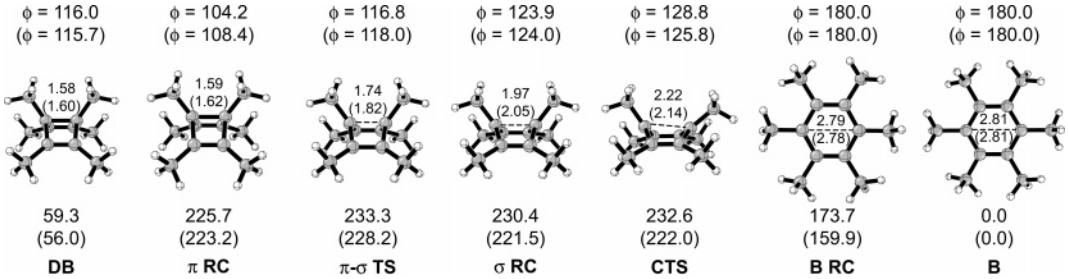

Figure 4. UB3LYP/6-311+G(d,p) hexamethyl Dewar benzene structures with flap dihedral, ϕ, reported in degrees, C−C bond distances reported in Å, and energies reported in kcal/mol. CAS/6-31G(d) values are shown in parentheses.

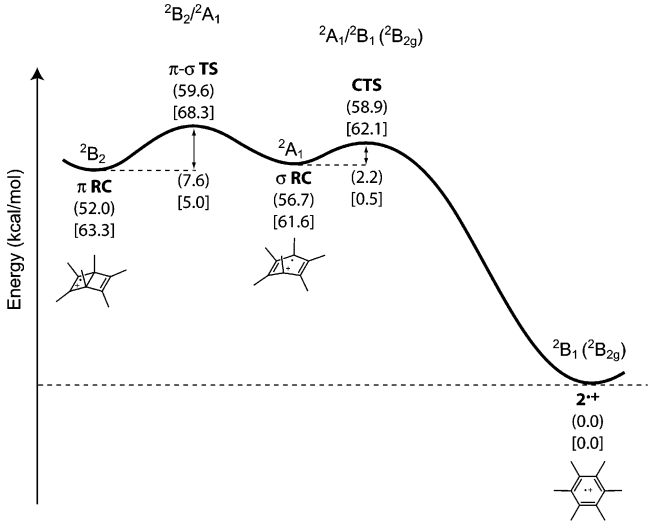

Figure 5. Potential energy surface for hexamethyl Dewar benzene radical cation with UB3LYP/6-311+G(d,p) values shown in parentheses and CAS/6-31G(d) values shown in brackets. Energies are reported in kcal/mol.

pathway leading almost exclusively to the strained trans conformation rather than **2**. Due to steric effects of the methyl groups, a preference for the disrotatory pathway is not observed. Due to interplay of steric effects of the methyl substituents and potential bond weakening and interaction between electronic states resulting from radical cation formation, it was not readily apparent whether to expect isomerization of the radical cation to occur via a conrotatory or disrotatory pathway. We provide evidence that, in fact, conversion of $\mathbf{1}^{\bullet+}$ into $\mathbf{2}^{\bullet+}$ occurs through an asymmetric transition state that breaks the plane of symmetry that defines the disrotatory pathway. An entirely equivalent way of looking at this reaction is provided by BMB upon discovery that the ground state of $\mathbf{3}^{\bullet+}$ strongly interacts with low-lying excited states. In this sense, the mechanism of the ring opening of $\mathbf{1}^{\bullet+}$ and $\mathbf{3}^{\bullet+}$ proceeds through crossings between surfaces of different symmetry, making it more evident as to how two minima exist.

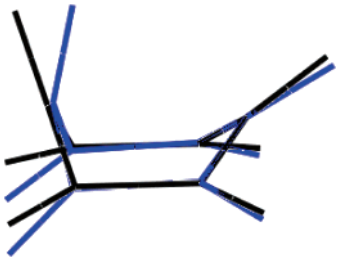

Figure 6. Best-fit overlay of (U)B3LYP/6-311+G(d,p) conrotatory ring-opening structures for Dewar benzene radical cation **CTS** (black) and neutral Dewar benzene (blue), by superimposing the positions of the carbon atoms (RMSD = 0.044 Å). The structural similarities, as well as the similarities in MOs suggest that **CTS** is a true conrotatory transition state rather than a disrotatory transition state that is merely asymmetric.

From σ **RC**, the radical cation proceeds to the fully planar $\mathbf{2}^{\bullet+}$ via a conrotatory-like transition structure, **CTS**. The imaginary frequency for this structure corresponds to the final step of ring opening and involves an asymmetric motion where one carbon of the transannular C−C bond exhibits a strong outward flapping motion. A very small activation barrier of 2.2 kcal/mol for **1** and 1.2 kcal/mol for **3** at (U)B3LYP/6-311+G(d,p) exists for this TS from σ **RC**. These barriers are essentially nonexistent using CAS/6-31G(d) unless state averaging over the lowest two roots is considered. The barrier then becomes 2.6 kcal/mol for **1** and 1.7 kcal/mol for **3**. The activation energies obtained from the two transition states $\pi-\sigma$ **TS** and **CTS** are, in general, quite similar. In fact, based on CCSD(T)/cc-pVTZ single-point energy calculations of B3LYP structures of **3** reported by BMB, the energy barrier for CTS is actually larger than $\pi-\sigma$ **TS**.

The conrotatory ring-opening transition structures (**CTS**) for Dewar benzene and its radical cation were compared at the (U)-B3LYP/6-311+G(d,p) level of theory. A best-fit superimposition of the carbon atoms shown in Figure 6 reveals that the carbon skeleton of the conrotatory structures are fundamentally similar (RMSD = 0.044 Å). The most notable difference is the larger pyramidalization angle for the inward-rotating CH group,

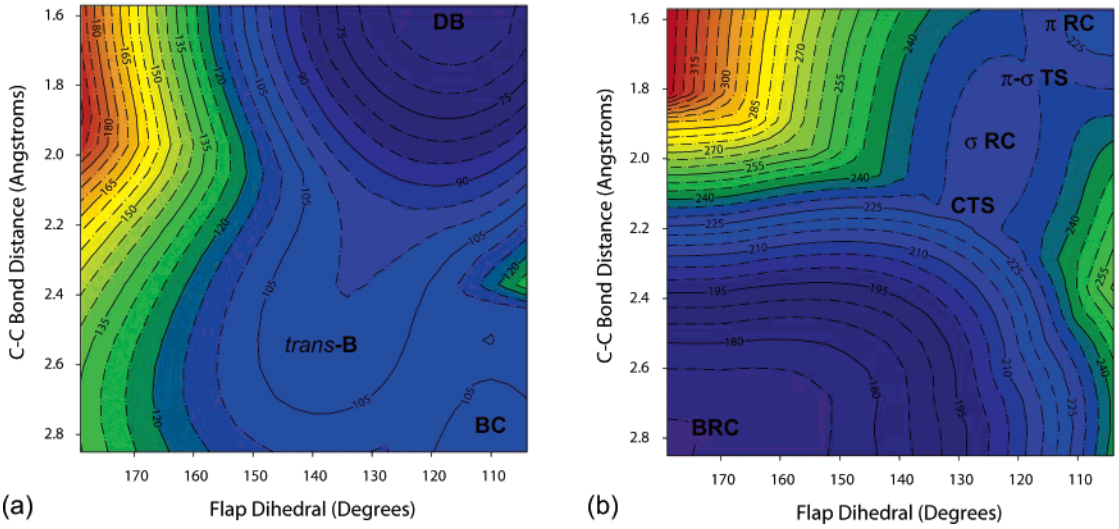

Figure 7. Contour plots of the (a) neutral (RB3LYP/6-31G(d)) and (b) radical cation (UB3LYP/6-31G(d)) potential energy surfaces of hexamethyl Dewar benzene **1**. Energies are reported in kcal/mol.

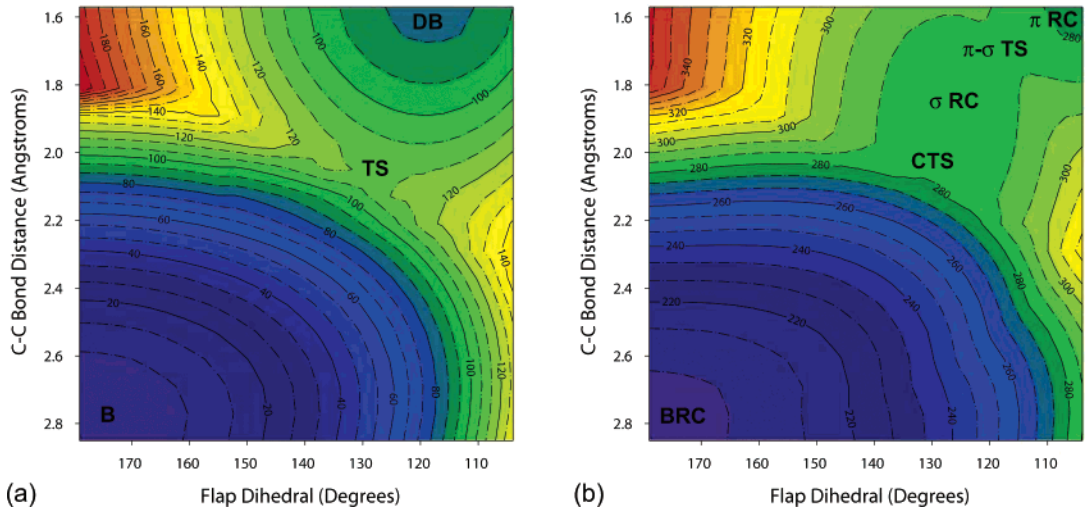

Figure 8. Contour plots of the (a) neutral (RB3LYP/6-31G(d)) and (b) radical cation (UB3LYP/6-31G(d)) potential energy surfaces of the Dewar benzene parent system **3**. Energies are reported in kcal/mol.

affecting the position of the hydrogen. The angle formed by the hydrogen, carbon, and a point midway between the two carbon atoms bonded to the first carbon is 26.6° for the neutral structure and 4.2° for the radical cation. Examination of the orbitals of the two species shows that the same molecular orbitals are involved, suggesting that orbital symmetry is not an explanation for this pyramidalization difference. The electrostatic potential (ESP) fit charges of **CTS** reveal that the carbon atom of the inward-rotating CH group bears more positive charge than any of the other carbons in this radical ion, so this is probably just a planar-carbocation effect. The interpretation from this comparison is that, although **CTS** has an appearance that is less obviously conrotatory than the neutral species, the same orbital symmetry is likely to be involved.

The two main reaction coordinates for isomerization of **1** are along the transannular C−C bond and the flap dihedral, ϕ. A two-dimensional surface scan along these coordinates was performed for the neutral (RB3LYP/6-31G(d)) and radical cation (UB3LYP/6-31G(d)) states of **1** and **3**. Contour plots of the surfaces of **1** are shown in Figure 7. The neutral ground-state surfaces for **1** and **3** are significantly different. The ring opening from **3** leads directly to benzene (Figure 8a), whereas the ring opening from **1** leads to the strained trans conformation (***trans*-B**) of hexamethylbenzene, rather than the planar conformation. Additional distortion along these coordinates in **1** even leads to a bicyclic diradical structure (**BC**). Open-shell calculations on initially calculated closed-shell structures of **BC** give lower energies because of the diradical electronic structure of the **BC** species. It should be noted that relative energies shown in Figure 7a correspond to restricted wave functions and that unrestricted energies for **BC** are lower; the energy well that **BC** lies in is not quite as shallow as that depicted in the contour plot.

Two observations become more apparent from the potential energy surfaces of the radical cations. First, the two minima, π **RC** and σ **RC**, sit in very shallow potential energy wells, which allows for significant structural flexibility. Second, transition states, $\pi-\sigma$ **TS** and **CTS**, actually exist on sharp ridges that are formed by avoided crossings connecting the three minima, which explains why these transition states were difficult to locate. This is also pointed out by BMB in conducting two-dimensional surface scans of **3**. The different levels of theory used here were consistent and gave little variation in the nature

of the critical points. The only significant discrepancy is in the asymmetry of **CTS**. This can be examined by looking at the two C−C−H bond angles involving the transannular C−C bond. UB3LYP/6-311+G(d,p) calculates C−C−H angles of 112.3° and 138.6°, and CAS/6-31G(d) calculates C−C−H angles of 122.7° and 129.5°. DFT predicts a more asymmetric conratatory-like **CTS** structure than that predicted by using the CASSCF method.

The location of the critical points on the surfaces shown in Figures 7 and 8 are helpful in understanding some factors that might limit the quantum efficiency of **1**. For example, the radical cation of hexamethyl Dewar benzene is known to undergo back-electron transfer from the photoinitiator, which should decrease quantum efficiency. However, **1** still isomerizes approximately half the time, indicating a coupling between isomerization and electron transfer. From the calculated surfaces, σ **RC** and **CTS** on the radical cation surface lie almost directly above the TS on the neutral surface, suggesting that if back-electron transfer were to occur in σ **RC**, relaxation on the ground state could lead to isomerization.

In reference to observed changes in ϕ, Kiau et al.[34] previously found that a significant decrease in the flap dihedral angle of **1** occurs upon removal of an electron from the π system. This was attributed to removal of an electron from a HOMO that has an antibonding combination between the two ethylene π orbitals. The radical cation surface calculated in our current study shows that initial oxidation of **1** occurs at the π bonds, resulting in π **RC**, where a π orbital is singly occupied and ϕ decreases. This species can isomerize to σ **RC** via $\pi-\sigma$ **TS** where the transannular σ bond is elongated and ϕ increases. In σ **RC**, ϕ increases to a value very close to that of neutral hexamethyl Dewar benzene, verifying that changes in ϕ are related to the singly occupied antibonding π orbital, as suggested by Kiau et al.[34]

In the isomerization of $\mathbf{1}^{\bullet+}$ to $\mathbf{2}^{\bullet+}$, two avoided crossings have been encountered, indicating that true state crossings should occur at slightly higher energies. It has been shown for systems such as radical cations, where the difference in energy between the ground state and first excited state is small, that location of conical intersections (CI) can be useful in characterizing reaction pathways.[22,59−61] The shape of the state-crossing regions of $\mathbf{1}^{\bullet+}$ alters the topology of the potential energy surface and is essentially responsible for the existence of two stable minima. This is an indication that the energy moats surrounding at least two state crossings contribute to the overall shape of the potential energy surface. According to orbital and state correlation arguments presented by BMB, a third crossing corresponding to intersection of the $^2B_2$ and $^2A_1$ states must also exist, though it is not clear that it is of relevance to the reaction under investigation. The CI corresponding to this crossing and the associated transition state have been found and discussed by BMB.

The two conical intersections (CI) corresponding to the $^2B_2/^2A_1$ (**CI ($\pi-\sigma$)**) and $^2A_1/^2B_1$ ($^2B_{2g}$) (**CI (CTS)**) state crossings of Dewar benzene and hexamethyl Dewar benzene have been

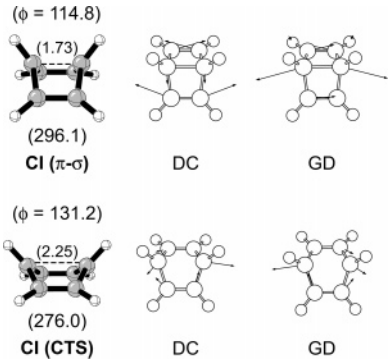

Figure 9. CAS(5,6)/6-31G(d) radical cation CIs for Dewar benzene. $\pi-\sigma$ CI most closely resembles $\pi-\sigma$ TS, and **CTS CI** most closely resembles **CTS**. The nonadiabatic derivative coupling (DC) and gradient difference (GD) vectors are shown. Flap dihedral, ϕ, is reported in degrees, C−C bond distances are reported in Å, and energies are reported in kcal/mol.

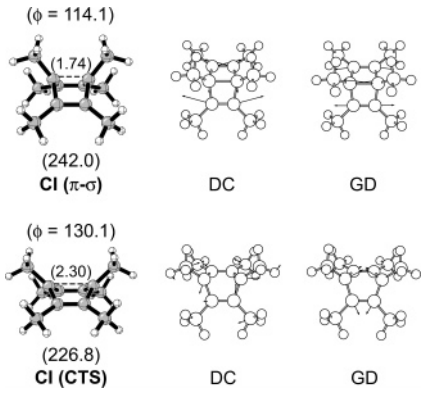

Figure 10. CAS(5,6)/6-31G(d) radical cation CIs for hexamethyl Dewar benzene. $\pi-\sigma$ CI most closely resembles $\pi-\sigma$ TS, and **CTS CI** most closely resembles **CTS**. The nonadiabatic derivative coupling (DC) and gradient difference (GD) vectors are shown. Flap dihedral, ϕ, is reported in degrees, C−C bond distances are reported in Å, and energies are reported in kcal/mol.

located and are shown in Figures 9 and 10. **CI ($\pi-\sigma$)** is the state crossing between π **RC** (C_{2v}) and σ **RC** (C_{2v}) and, consequently, structurally resembles $\pi-\sigma$ **TS**. **CI (CTS)** is the state crossing between σ **RC** and **BRC** (D_{2h}) and, similarly, resembles **CTS**. There are very few geometric differences between **CI ($\pi-\sigma$)** and $\pi-\sigma$ **TS**. For example, for **1**, **CI ($\pi-\sigma$)** exhibits a shortening of the bridge from 1.82 Å in $\pi-\sigma$ **TS** to 1.74 Å, and the flap dihedral decreases from 118.0° to 114.1°. In addition, the nonadiabatic derivative coupling (DC) and gradient difference (GD) vectors indicate movement of the π-bonded carbons, downward motion of the bridge carbons, and changes in the transannular C−C bond length. The movement of the π bonds occurs asymmetrically such that as one π bond shortens the other lengthens, and this is exhibited by nonequivalent π bond distances in $\pi-\sigma$ **TS**.

Closer analysis of these structures shows that **CI (CTS)** distinguishes itself from **CTS** by a longer bridge length, larger flap dihedral, and a less conrotatory-like structure, thereby, making it more planar. For **1**, **CI (CTS)** has a bridge length of 2.30 Å and flap dihedral angle of 130.1°, and **CTS** has a corresponding length of 2.14 Å and angle of 125.8°. Given that the descent toward **BRC** is extremely steep, it may be reasonable that lengthening of the bridge and flattening of the π system places the state crossing below π **RC** in energy. This is consistent with the fact that CASSCF predicts that **CI (CTS)** actually lies 3.6 kcal/mol below π **RC** and 15.2 kcal/mol below

(59) Blancafort, L.; Adam, W.; González, D.; Olivucci, M.; Vreven, T.; Robb, M. A. *J. Am. Chem. Soc.* **1999**, *121*, 10583−10590.
(60) Blancafort, L.; Jolibois, F.; Olivucci, M.; Robb, M. A. *J. Am. Chem. Soc.* **2001**, *123*, 722−732.
(61) Fernández, E.; Blancafort, L.; Olivucci, M.; Robb, M. A. *J. Am. Chem. Soc.* **2000**, *122*, 7528−7533.

Scheme 3 [a]

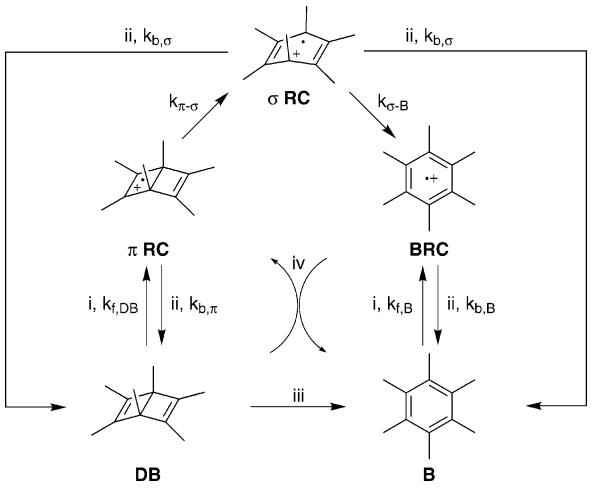

[a] (i) *hν*/sensitizer, (ii) back-electron transfer, (iii) Δ, (iv) hole transfer.

CI ($\pi-\sigma$). Similarly for **3**, **CI (CTS)** lies 2.9 kcal/mol below π **RC** and 20.1 kcal/mol below **CI ($\pi-\sigma$)**. Even though **CI (CTS)** appears to have less conrotatory character, DC and GD show that degeneracy between the two states is broken along coordinates involving conrotatory motion. As discussed, the natures of both CIs are very much like those of the corresponding transition structures found at the avoided crossings due to closely interacting electronic surfaces.

Electron Transfer and Propagation. Oxidation of reactant molecules by radical cation product molecules is a key step in the QAI mechanism. In order for this process to be efficient, the oxidized reactants should not readily undergo back-electron transfer, and the isomerized products should be able to undergo hole transfer to oxidize reactant molecules. Accordingly, analysis of charge transfer can be used to evaluate the efficiency of the QAI mechanism, assuming that diffusion and solvation of ion radicals occur readily. Specific electron-transfer events for the isomerization of **1** are depicted in Scheme 3 as irreversible and kinetically controlled events including back-electron transfer to the radical cation and hole transfer between isomerized radical product and reactant. These specific events can be considered using electron-transfer theory and parameters obtained from computational methods such as reorganization energies, redox potentials, and molecular volumes.[62−68] Compound **1** is treated with the use of electron-transfer theory, assuming close contact between the molecules. A two-mode vibrational model that incorporates low-frequency polarization modes of the solvent and high-frequency skeletal vibrations of the donor and acceptor molecules has been used to analyze electron transfer, as shown in eq 1.[39−47] Reorganization energy of the solute, ionization energies, and electron affinities are calculated using quantum mechanics.

The propagation step, i.e., electron transfer between the benzene radical cation and Dewar benzene, plays a critical role in determining the amplification of isomerization. Propagation is shown as the last step of the QAI process depicted in Scheme 2. For a driving force for electron transfer to occur, one would expect the radical cation of the product to have an electron affinity greater than the ionization energy of the neutral reactant. Ionization energies of the neutral reactants ($IE_{reactant}$) and electron affinities of the radical cation products ($EA_{product\bullet+}$) were calculated at the CAS/6-31G(d), (U)B3LYP/6-31G(d), and (U)-B3LYP/6-311+G(d,p) levels of theory and are reported in Table 3.

In terms of electron-transfer theory, adiabatic transitions correspond to the thermodynamic driving force of the reaction and, therefore, are the values of interest when considering oxidation and reduction. For comparison, both vertical and adiabatic values of reactants **1**, **3**, **5**, **7**, **9**, and **11**, and products **2**, **4**, **6**, **8**, **10**, and **12** are reported in Table 3. The adiabatic $IE_{reactant}$ and $EA_{product\bullet+}$ values for the reactions of **1** and **3** suggest that the benzene radical cation is able to oxidize Dewar benzene. DFT methods predict adiabatic $EA_{product\bullet+}$ values to be ∼0.5 eV larger than $IE_{reactant}$ values for **3** and ∼0.3 eV larger for **1**. Even though it is desirable for the cation of the ring-opened product to have a high EA so that it can readily remove an electron from a reactant molecule, an EA that is too high will promote efficient return electron transfer from the sensitizer, thereby terminating the QAI reaction. Likewise, if the oxidation potential of the sensitizer is small, this would promote back-electron transfer from the sensitizer to the radical cation. This implies that some tuning of the QAI reaction could be important or that one would have to use a sensitizer whose radical anion rapidly rearranges to something less readily oxidized.

The molecules studied here, with the exception of **5**, have reorganization energies ≤0.6 eV, and all have vertical $IE_{reactant}$ values greater than the vertical $EA_{product\bullet+}$ values of their isomerized cation products. Again, adiabatic transitions are of interest here and result in transitions consistent with amplification of isomerization. For experimentally studied systems **1**, **5**, and **7**, $IE_{reactant}$ is calculated to be lower than or approximately equal to $EA_{product\bullet+}$. For isomerization of **1** to **2**, adiabatic $IE_{reactant}$ and $EA_{product\bullet+}$ values are calculated to be 7.03 and 7.35 eV, respectively, and 8.41 and 8.86 eV for the parent system **3**. The corresponding values for **5** are 6.49 and 6.76 eV, and 6.80 and 6.78 eV for **7**.

We also considered two potential QAI systems—a well-known photochromic system, diethienylethene (**9**), and a benzocyclobutene derivative (**11**) currently being studied in the Houk Group for potential molecular-switch applications, and both are shown in Figure 2. Structure **9** has a low reorganization energy (0.17 eV), a vertical $EA_{product\bullet+}$ value that is ∼0.5 eV greater than its vertical $IE_{reactant}$ value, and an adiabatic $EA_{product\bullet+}$ value almost a full eV greater than its adiabatic $IE_{reactant}$ value. In the ground state, the ring opening of **9** is a Woodward−Hoffmann-forbidden process, and the forbidden nature of this process is still evident for the radical cation, which is predicted to have an activation barrier of 26 kcal/mol. This forbidden ring opening makes **9** unfavorable for QAI. Structure **11** is predicted to have low reorganization energy (0.08 eV) and has a barrier for ring opening of approximately 1 kcal/mol for the radical cation. However, vertical and adiabatic $EA_{product\cdot+}$ values are considerably lower than its $IE_{reactant}$ value, indicating that amplification would not be expected to occur via oxidation by the radical cation product.

(62) Kurnikov, I. V.; Beratan, D. N. *J. Chem. Phys.* **1996**, *105*, 9561−9573.
(63) Kurnikov, I. V.; Zusman, L. D.; Kurnikova, M. G.; Farid, R. S.; Beratan, D. N. *J. Am. Chem. Soc.* **1997**, *119*, 5690−5700.
(64) Liang, C.; Newton, M. D. *J. Phys. Chem.* **1993**, *97*, 3199−31211.
(65) Lin, B. C.; Cheng, C. P.; Lao, Z. P. M. *J. Phys. Chem. A* **2003**, *107*, 5241−5251.
(66) Newton, M. D. *Chem. Rev.* **1991**, *91*, 767−792.
(67) Todd, M. D.; Nitzan, A.; Ratner, M. A. *J. Phys. Chem.* **1993**, *97*, 29−33.
(68) Jordan, K. D.; Paddon-Row: M. N. *Chem. Rev.* **1992**, *92*, 395−410.

Table 3. Calculated Reorganization Energies (λ_D), Ionization Energies (IE), and Electron Affinities (EA) at (U)B3LYP/6-31G(d)[a]

		(U)B3LYP/6-31G(d)				(U)B3LYP/6-311+G(d,p)			
		vertical		adiabatic		vertical		adiabatic	
reaction[b]	λ_D	$IE_{reactant}$	$EA_{product^{\bullet+}}$	$IE_{reactant}$	$EA_{product^{\bullet+}}$	$IE_{reactant}$	$EA_{product^{\bullet+}}$	$IE_{reactant}$	$EA_{product^{\bullet+}}$
1 → **2**	0.46	7.40	7.15	7.03	7.35	7.59	7.33	7.22	7.53
3 → **4**	0.57	8.85	8.71	8.41	8.86	9.11	8.99	8.68	9.13
5 → **6**	1.45	7.30	6.55	6.49	6.76				
7 → **8**	0.19	6.96	6.64	6.80	6.78				
9 → **10**	0.17	6.75	7.28	6.54	7.50				
11 → **12**	0.08	7.21	5.43	7.13	5.54				

[a] Energies are reported in eV. [b] Experimental vertical ionization energies for **1** and **3** are 7.8 and 9.4 eV, and corresponding experimental values for **2** and **4** are 7.85 and 9.25 eV, respectively.[72,73]

Two stable radical cation minima, π **RC** and σ **RC**, are predicted to exist upon oxidation of **1** and could have potential effects on back-electron transfer in the isomerization of **1** to **2**. The energy barrier for conversion of π **RC** to σ **RC** is predicted to be significant enough to compete with electron-transfer events. In contrast, the calculated activation energy for isomerization of σ **RC** to **2** is small (2.2 or 0.5 kcal/mol) and suggests that σ **RC** will quickly isomerize to **2**. Electron-transfer theory and transition-state theory have been applied to compare relative rates of isomerizaiton and back-electron transfer.

The parameters in eqs 1 and 2 must be obtained computationally or from experiments to analyze electron-transfer. Exciplexes involving cyanoaromatic acceptors and methylbenzene donors have been reported to have coupling matrix element, V, values of ~0.1 eV.[69−71] Electron-transfer rates are calculated assuming $\nu = 1400\ cm^{-1}$ for high-frequency skeletal vibrations of the donor and acceptor. Solvent reorganization energy, λ_s, was calculated to be 0.56 eV for both **1** and **2**, according to Marcus theory.[39,40] Vibrational reorganization energies, λ_D, for solutes **1** and **2** were determined from calculations to be 0.46 and 0.21 eV, respectively. If the reorganization energy is taken as the difference between vertical and adiabatic ionization energies, λ_D for **1** can be approximated from its photoelectron spectrum as the difference between band onset and the maximum of the first photoelectron band, which is about 0.4 eV and in general agreement with the calculated value.[72,73] Various cyanonaphthalenes have been used as electron acceptors in electron-transfer reactions of hexametheyl Dewar benzene.[34] For the purpose of this study, 2-cyanonaphthalene, which has a reduction potential of −1.98 eV and a singlet excitation energy of 3.83 eV, was chosen as a general electron acceptor, for which λ_A was calculated to be 0.14 eV, giving a total vibrational energy, λ_v, of 0.60 eV for **1** and 0.35 eV for **2**. Of course different acceptors will have slightly different reorganization energies and reduction potentials, but 2-CN is used here as a model electron acceptor.

Redox potentials were obtained from the computationally determined ΔG values using procedures developed previously for small molecules in solution.[74−76] Given that ΔG values are known to be underestimated using the 6-31G(d) basis set, additional polarization and diffuse functions included by the 6-311+G(d,p) basis set only slightly underestimate these values. The experimental vertical ionization energies of **1** and **3** are 7.8 and 9.4 eV, respectively.[72] B3LYP/6-31G(d) underestimates these values by 0.3−0.4 eV, whereas B3LYP/6-311+G(d,p) underestimates them by only 0.1−0.2 eV. The experimental vertical ionization energies for the associated benzene molecules **2** and **4** are 7.85 and 9.25 eV respectively, and are underestimated by 0.2−0.6 eV using the 6-31G(d) basis set and by up to 0.3 eV using the 6-311+G(d,p). Some cancellation of errors should occur since the vertical ionization energies of both the Dewar benzene and benzene systems are underestimated by B3LYP. The use of diethyl ether ($\epsilon = 4.335$, $n = 1.3542$) as the solvent has been reported in electron-transfer studies of hexamethyl Dewar benzene[34] and, therefore, is used as the solvent for calculating ΔG values. These values along with the reorganization energies are reported in Table 4. The rates calculated from eqs 1 and 2 are reported in Table 5.

Table 4. Solvent Reorganization Energies, λ_s, and Donor (λ_D), Acceptor (λ_A) (2-CN), and Total (λ_v) Vibrational Reorganization Energies of the Solute Were Calculated at B3LYP/6-31G(d);[a] Standard Redox Potentials, E^0, Were Calculated at B3LYP/6-311+G(d,p)[b]

	λ_s	λ_D	λ_A	λ_v	E^0	ΔG_f	ΔG_b
1	0.56	0.46	0.14	0.60	1.66	−0.60	−3.23
2	0.56	0.21	0.14	0.35	2.03	−0.23	−3.60

[a] Calculated radii used for **1**, **2**, and 2-CN are 4.31, 4.25, and 3.88 Å, respectively. [b] All values are reported in eV

Table 5. Rates for Forward (k_f)- and Back (k_b)-Electron Transfer as Calculated from eqs 2 and 3; Rate Constants for Interconversion between the Different Stationary Points on the Radical Cation Surface of **1** as Determined by eq 9

	k_f	k_b	$k_{\pi-\sigma}$[a]	$k_{\sigma-B}$
1	1.06×10^{14}	9.96×10^{10}	1.64×10^{7}	1.55×10^{11}
2	1.15×10^{14}	2.09×10^{7}		

[a] Calculated from the Eyring equation in ref 77 using an activation energy of 7.6 kcal/mol obtained using UB3LYP/6-311+G(d,p). If the CAS/6-31G(d) activation energy of 5.0 kcal/mol is used, $k_{\pi-\sigma} = 1.34 \times 10^9$.

From the electron-transfer rates calculated here, there is an apparent difference between forward-electron transfer (k_f) and back-electron transfer (k_b). Forward-electron transfer is rapid for both **1** and **2**, on the order of $10^{14}\ s^{-1}$, which is greater than

(69) Gould, I. R.; Noukakis, D.; Gomez-Jahn, L.; Young, R. H.; Goodman, J. L.; Farid, S. *Chem. Phys.* **1993**, *176*, 439−456.
(70) Gould, I. R.; Noukakis, D.; Goodman, J. L.; Young, R. H.; Farid, S. *J. Am. Chem. Soc.* **1993**, *115*, 3830−3831.
(71) Gould, I. R.; Young, R. H.; Moody, R. E.; Farid, S. *J. Phys. Chem.* **1991**, *95*, 2068−2080.
(72) Bieri, G.; Heilbronner, E.; Kobayashi, T.; Schmelzer, A.; Goldstein, M. J.; Leight, R. S.; Lipton, M. S. *Helv. Chim. Acta* **1976**, *59*, 2657−2673.
(73) Bieri, G.; Heilbronner, E.; Goldstein, M. J.; Leight, R. S.; Lipton, M. S. *Tetrahedron Lett.* **1975**, 581−584.
(74) Dutton, A. S.; Fukuto, J. M.; Houk, K. N. *Inorg. Chem.* **2005**, *44*, 4024−4028.
(75) Baik, M.-H.; Friesner, R. A. *J. Phys. Chem. A* **2002**, *106*, 7407−7412.
(76) Redox potentials were calculated from the Nernst equation using ΔG_{gas}, the sum of electronic and thermal free energies at 298 K, and ΔG_{solv}, the calculated free energy of solvation. A detailed description of this procedure and the methods used is provided in the Supporting Information.

Table 6. Refractive Indices Calculated Using Static and Frequency-Dependent (λ = 632 nm) Isotropic Polarizabilities[a]

			static			632 nm		
	mol vol (Å^3/mol)	N (mol/Å^3)	$\alpha(\omega)$ (bohr^3)	$n(\omega)$	Δn	$\alpha(\omega)$ (bohr^3)	$n(\omega)$	Δn
			B3LYP/6-31G(d)					
1	335.68[b]	0.002979	120.60	1.3642		123.29	1.3733	
2	316.99	0.003155	126.85	1.4112	0.0470	130.90	1.4262	0.0529
3	139.91	0.007148	52.49	1.3823		53.58	1.3912	
4	148.46[b]	0.006736	54.50	1.3731[c]	−0.0092	56.17	1.3859[c]	−0.0053
5	575.52	0.001738	228.99	1.4085		236.18	1.4232	
6	592.81	0.001687	237.46	1.4116	0.0031	247.43	1.4314	0.0083
7	738.82	0.001354	279.78	1.3863		289.28	1.4011	
8	760.71	0.001315	316.86	1.4304	0.0441	342.61	1.4711	0.0700
9	548.98	0.001822	220.44	1.4128		269.27	1.5209	
10	581.83	0.001719	202.42	1.3514	−0.0614	209.44	1.3650	−0.1559
11	544.77	0.001836	251.34	1.4846		264.38	1.5144	
12	537.91	0.001859	351.56	1.7458	0.2612	95.34	1.1708	−0.3435
			B3LYP/6-311+G(d,p)					
1	335.68[b]	0.002979	138.54	1.4259		142.22	1.4389	
2	316.99	0.003155	143.98	1.4758	0.0499	149.02	1.4954	0.0565
3	139.91	0.007148	63.03	1.4712		64.80	1.4868	
4	148.46[b]	0.006736	66.16	1.4653[c]	−0.0059	68.66	1.4859[c]	−0.0008

[a] Molecular volumes obtained using the GRASP program[53,54] unless otherwise stated. [b] Molecular volumes obtained from experimental densities from the Sigma-Aldrich database. [c] n (λ = 590 nm) = 1.5011.[83]

typical diffusion control rates that are on the order of 10^{10} M^{-1} s^{-1}. The rate for back-electron transfer for **2**$^{\bullet+}$ is predicted to be on the order of 10^7 s^{-1}, which is significantly slower than k_f and an indication that **2**$^{\bullet+}$ should persist long enough to oxidize **1**. More importantly, k_b for **1**$^{\bullet+}$ is calculated to be on the order of 10^{10} s^{-1}, which is faster than the rate-limiting step ($k_{\pi-\sigma}$ = 1.64×10^7 s^{-1}) for conversion of **1** into **2** on the radical cation surface and, thus, is expected to compete significantly with radical cation isomerization, leading to a reduction in efficiency.[77] This could be, at least in part, as a result of the large (0.56 eV) reorganization energy calculated for **1**. Kiau et al. arrived at similar conclusions based on the emission spectra of excited-state electron acceptors with **1**.[34] Back-electron transfer is not expected to be competitive with conversion of the second radical cation, σ **RC**, to the fully isomerized system; the rate for isomerization from σ **RC** is on the order of 10^{11} s^{-1}.

Frequency-Dependent Index of Refraction. Organic imaging materials are known to rely on photoinduced electron transfer to generate free radicals or acids that initiate polymerization in molecularly doped polymeric media[78−80] and to induce reactions that cause changes in properties such as solubility.[81,82] Similarly, potential optical applications for systems exhibiting QAI rely on photoinduced reactions to cause contrasts in index of refraction between reactant and product. Given that index of refraction is a function of polarizability and the number of molecules-per-unit volume, transformations in π conjugation and/or volume would contribute to changes in refractive index. For example, the conjugated π system of hexamethylbenzene (**2**) is more polarizable than that of hexamethyl Dewar benzene (**1**), which has isolated double bonds, and because there is only a small volume difference, the refractive index goes up after isomerization. It has been shown that accurate refractive indices of aromatic systems can be calculated from electronic structure calculations of frequency-dependent polarizabilities.[51,52]

Indices of refraction determined from calculated static and frequency-dependent polarizabilities are listed in Table 6. For isomerization of **1** to **2**, B3LYP/6-31G(d) predicts a change from n = 1.3733 to n = 1.4262 at λ = 632 nm, giving Δn of 0.0529. B3LYP/6-311+G(d,p) predicts Δn = 0.0565 from n = 1.4389 to n = 1.4954. Changes in index of refraction of Δn = 0.004 have been experimentally measured for copolymers of **1**.[17−20] Measurements of the pure materials of **1** are difficult to measure since **2** is a solid. However, some ester-containing liquid derivatives have yielded Δn values between 0.040 and 0.045,[17−20] indicating that the calculated Δn values are reasonable. Interestingly, even though B3LYP/6-311+G(d,p) calculates benzene to have a greater $\alpha(\omega)$ than Dewar benzene, a negligible decrease in n (Δn = −0.0008) is predicted, suggesting that **1** is a better candidate for optical applications than **3**. B3LYP/6-31G(d) estimates **5** to be an order of magnitude poorer in terms of Δn than **1**, and **7** is expected to be comparable to **1**.

The photochromic dithienylethene (**9**) and benzocyclobutene (**11**) are both calculated to have Δn values an order of magnitude greater than **1**. The *o*-xylylene product (**12**) was determined earlier not to be a good oxidizing agent for the reactants and, therefore, would not lead to amplification. Alternatively, **10** is expected to have a greater EA than its closed-ring reactant (**9**), which has a low reorganization energy, an excellent change in refractive index, and well-known photochromic behavior. However, even though the ring opening of **9**$^{\bullet+}$ is endothermic by 8.5 kcal/mol, the activation energy is sufficiently high at 26.2 kcal/mol.

Conclusions

The radical cation states of Dewar benzene and its hexamethyl derivative have two transition states near avoided crossings that

(77) According to transition-state theory, the reaction rate constant k is defined as $k = (k_B T/h) \exp(-\Delta G^{\ddagger}/RT)$ where T is 298 K, and $\Delta G^{\ddagger}$, the free energy of activation, is approximated by the relative electronic energy of activation, $\Delta E^{\ddagger}$.

(78) Crivello, J. V. *NATO Adv. Study Inst. Ser., Ser. E: Appl. Sci.* **1999**, *359*, 45−60.
(79) Belfield, K. D., Crivello, J. V., Eds. *Photoinitiated Polymerization*; ACS Symposium Series 847; American Chemical Society: Washington, DC, 2003.
(80) Fouassier, J. P.; Rabek, J. F., Eds. *Radiation Curing in Polymer Science and Technology*; Elsevier: New York, 1993.
(81) Stewart, M. D.; Patterson, K.; Somervell, M. H.; Willson, C. G. *J. Phys. Org. Chem.* **2000**, *13*, 767−774.
(82) Reiser, A. *Photoreactive Polymers*; Wiley: New York, 1989.
(83) Lide, D. R., Ed. *CRC Handbook of Chemistry and Physics*, Internet Version; CRC Press: Boca Raton, FL, 2005.

connect two radical cation minima before fully isomerizing to the benzene radical cation. Two conical intersections corresponding to the avoided crossings have been located and are found to closely resemble the related transition states. Initial oxidation generates a radical cation that is protected by an activation barrier that leads to a less stable structure that will quickly rearrange to benzene with conrotatory stereochemistry. The potential energy surfaces of both **1** and its parent system are found to undergo broadening, which is due to bond weakening associated with radical cation structures.

The quantum amplification of isomerization relies on the ability of the radical cation product to oxidize reactant molecules. For **1**, calculated adiabatic ionization potentials and electron affinities verify that $\mathbf{2}^{\bullet+}$ is a suitable oxidizer for amplification, as are $\mathbf{6}^{\bullet+}$ and $\mathbf{8}^{\bullet+}$ for their neutral precursors **5** and **7**. Opened-ring dithienylethene $\mathbf{10}^{\bullet+}$ is predicted to oxidize closed-ring **9** but has a high activation energy for ring opening, whereas *o*-xylylene **12** is predicted to be unable to oxidize its closed-ring reactant. Electron-transfer theory was applied to **1** and predicts that back-electron transfer to $\mathbf{1}^{\bullet+}$ will compete with isomerization, although once isomerization occurs, $\mathbf{2}^{\bullet+}$ is expected to persist long enough to oxidize **1**.

Indices of refraction have been calculated for the various systems studied here and have been found to be a useful tool in evaluating changes in optical properties. Change in the refractive index for **1** is predicted to be significantly larger than for its parent system and **5**. However, **7** is expected to exhibit a change in refractive index comparable to that of **1**, while **9** is calculated to exhibit a large change.

The findings described here rely on hybrid DFT methods as tools for studying radical ion reactions. For Dewar benzene and hexamethyl Dewar benzene, where the actual pathway to the ring opening of the neutral state was unclear, calculations here and in the accompanying paper[55] have shown that radical cation isomerization involves a transition state with a conrotatory-like mode and no indication of disrotatory opening. One-electron transfer is shown here to be useful in controlling pericyclic reactions for applications in potential imaging systems.

Acknowledgment. We are grateful to the National Science Foundation (NSF) for financial support. This research was facilitated through the Partnerships for Advanced Computational Infrastructure (PACI) through the support of the NSF. Computations were performed on the NSF Terascale Computing System at the Pittsburgh Supercomputing Center (PSC) and on the UCLA Academic Technology Services (ATS) Hoffman Beowulf cluster. J.E.N. also acknowledges the Integrative Graduate Education and Research Traineeship program supported by the NSF at UCLA for financial support. We thank Dr. Douglas R. Robello for helpful discussions and for providing us with a copy of a poster presented at the Sixth International Symposium on Functional π-Electron Systems.[17]

Supporting Information Available: Details of computational procedure, Cartesian coordinates, and absolute energies for all calculated compounds at B3LYP/6-31G(d), B3LYP/6-311+G-(d,p), and CAS/6-31G(d); complete ref 35. This material is available free of charge via the Internet at http://pubs.acs.org.

JA060182I